Chaos, Solitons and Fractals 190 (2025) 115777

Contents lists available at ScienceDirect

Chaos, Solitons and Fractals

journal homepage: www.elsevier.com/locate/chaos

Vortex light bullets in rotating Quasi-Phase-Matched photonic crystals with quadratic and cubic nonlinearity

Shunfang Chen [a,b,1], Linjia Wang [a,c,1], Zhuo Fan [a,c], Wei Peng [a,c], Di Wu [a,c], Yuan Zhao [a,c,*], Siliu Xu [a,c,*]

[a] Key Laboratory of Optoelectronic Sensing and Intelligent Control, Hubei University of Science and Technology, Xianning, 437100, China
[b] School of Electronic and Information Engineering, Hubei University of Science and Technology, Xianning 437100, China
[c] School of Biomedical Engineering and Imaging, Xianning Medical College, Hubei University of Science and Technology, Xianning 437100, China

ARTICLE INFO

Keywords:
Vortex light bullets
Rotating Quasi-Phase-Matched photonic crystal
Competing quadratic and cubic nonlinearity

ABSTRACT

We design a setup for generating stable vortex light bullets (LBs) in a rotating Quasi-Phase-Matched (QPM) photonic crystal, exhibiting competing quadratic and cubic nonlinearity. The photonic crystal is designed with a rotational checkerboard structure. Within this framework, three types of vortex LBs (square-, rhombus- and necklace-shaped) are observed, which are constructed as four-peak and eight-peak vortex modes, respectively. The dynamics of vortex LBs are controlled by system parameters, including the power, rotating frequency, size of checkerboard cells, and azimuthal indices of the incident light. In contrast to the stable two-dimensional vortex solitons observed in pure quadratic systems, the vortex LBs investigated in the competing quadratic and cubic nonlinear system can support vortex LBs with higher topological charges. Especially, the rotating frequency results in a transition of vortex LBs from a quadrupole to the traditional vortex modes.

1. Introduction

Light bullets (LBs), localized wave packets that achieve a delicate equilibrium between diffraction, dispersion, and nonlinearity [1–3], have attracted considerable attention in recent years [4,5]. These unique wave packets hold pivotal significance in diverse applications, including communication and rapid data processing in optical systems [6–9], as well as quantum droplets in Bose–Einstein condensates [10,11]. However, the generations of three-dimensional (3D) LBs face a significant challenge compared to their low-dimensional counterparts. The primary obstacle arises from the inherent cubic, locally self-attracting nonlinearity that triggers critical and supercritical collapses of LBs in higher dimensions [12–17]. Moreover, the experimental realization of LBs faces numerous difficulties. One prominent challenge is achieving a balance with random noise [18,19]. Among these LBs, vortex LBs have attracted particular interest due to their possession of nonzero angular momentum, a feature that notably contributes to their pronounced azimuthal instability [20,21].

Over the past two decades, LBs have been studied both theoretically and experimentally. The first experimental observation of LBs was reported in 1999 through the cascaded second harmonic generation process in bulk media [22]. Subsequently, 2D LBs in LiIO3 crystals [23] and quasi-3D LBs in waveguide arrays [24] were discovered. More recently, Lahav et al. reported trains of 3D dark solitons in photorefractive materials [25]. However, these LBs often suffer from severe instability, limiting their propagation to just a few diffraction lengths. Theoretically, numerous setups have been proposed to investigate the formation and dynamics of LBs. To stabilize LBs, researchers have explored various nonlinear optical materials, including those with spatially patterned nonlinear interactions [26], optical tandem systems [27], materials exhibiting saturable, competing, or nonlocal nonlinearities [28,29], hybrids of local and nonlocal nonlinearities [30,31], and combinations of quadratic and cubic nonlinearities [32–34].

Another effective approach for achieving stable LBs involves spatial modulation of optical lattices. Stable vortices have been predicted in 2D lattices with cubic nonlinearity [35,36]. Stable LBs can form in both discrete [37,38] and continuous [39,40] lattices, even when the input beams carry vorticity [41–43]. Notably, the Rydberg electromagnetically induced transparency (Rydberg-EIT) system has emerged as an effective medium for generating stable LBs due to the nonlocal nonlinearities arising from the long-range Rydberg–Rydberg interactions [44–48].

In recent years, Quasi-Phase-Matched (QPM) crystals have attracted a lot of attentions due to their ability to facilitate the generation of

* Corresponding authors.
E-mail addresses: yuanuanz@163.com (Y. Zhao), xusiliu1968@163.com (S. Xu).
[1] The authors contributed equally in this work.

https://doi.org/10.1016/j.chaos.2024.115777
Received 30 September 2024; Received in revised form 31 October 2024; Accepted 15 November 2024
Available online 27 November 2024

quadratic nonlinearity within the medium [49–51], thereby enabling the production of stable 2D vortex solitons [52]. Distinguishing themselves from vortex solitons in spatially uniform quadratic systems, which are inherently unstable, these recently discovered families exhibit remarkable stability across extensive regions within the system parameter space. In this system, tightly bound rhombic vortex solitons occupy the ground state of system, which is characterized by the minimal Hamiltonian and a more wider stability range compared to loosely bound square solitons. Further, stable vortex LBs were found in a rotational QPM crystal with quadratic nonlinearity [53].

Despite the above progress, 3D vortex LBs created in a combination of quadratic and cubic nonlinearity are still inadequately understood, especially in a rotating coordinate system. This paper aims to construct 3D stable vortex LBs in a rotating QPM photonic crystal with competing quadratic and cubic nonlinearity. Following the work [52,53], we design a setup for generating stable vortex LBs using high-power optical beams in a rotating system. This technique is based on spatial modulation of quadratic and cubic nonlinearity, which is achieved by means of periodic poling of the crystalline material [54–57] in 2D and the femtosecond laser engineering technology in 3D system [58,59]. We find three kinds of vortex LBs (square-, rhombus- and necklace-shaped), which are constructed as four-peak and eight-peak vortex modes with different topological charges. Control parameters include the azimuthal indices of the incident light, power, angular velocity of rotation, and the size of each square cell. These parameters affect the distribution and stability range of these vortex LBs. In particular, the rotating frequency results in the transition of vortex LBs from a quadrupole to the traditional vortex modes.

2. The model

We elaborate on a mechanism for stabilizing vortex LBs using a 3D QPM nonlinear photonic crystal, where electric fields with fundamental-frequency (FF) and second-harmonic (SH) modes propagate along the z direction [60]

$$\mathbf{E}_{1,2}(\mathbf{r},t)=\frac{1}{2}\hat{e}A_{1,2}\exp\left[i(k_{1,2}Z-\omega_{1,2}t)\right]+\text{c.c.}, \tag{1}$$

where the indices 1 and 2 represent the FF and SH modes, respectively; $\mathbf{r}=(X,Y)$, Z and t are the transverse, longitudinal, and time coordinates; $A_{1,2}$, $k_{1,2}$, and $\omega_{1,2}$ are, respectively the envelope, wave-vector, and frequency of light fields; c.c. is the complex conjugate. In this work, the light field propagates in Z direction, and the frequencies of FF and SH modes satisfy $\omega_2=2\omega_1=2\omega$.

Using a standard procedure and applying the paraxial and slowly varying envelope approximations [60], the envelops $A_{1,2}(\mathbf{r},t)$ are governed by the following coupled equations:

$$\begin{aligned}
&i\frac{\partial A_1}{\partial Z}-\frac{K}{2}\frac{\partial^2 A_1}{\partial T^2}+\frac{1}{2k_1}\left(\frac{\partial^2 A_1}{\partial X^2}+\frac{\partial^2 A_1}{\partial Y^2}\right)+\frac{\pi\omega_1\chi^{(2)}}{2cn_1}A_1^*A_2e^{-i\Delta k_0 Z}\\
&\quad+\frac{\pi 3\omega_1\chi^{(3)}}{2cn_1}\left(|A_1|^2+2|A_2|^2\right)A_1=0,\\
&i\frac{\partial A_2}{\partial Z}-\frac{K}{2}\frac{\partial^2 A_2}{\partial T^2}+\frac{1}{2k_2}\left(\frac{\partial^2 A_2}{\partial X^2}+\frac{\partial^2 A_2}{\partial Y^2}\right)+\frac{\pi\omega_2\chi^{(2)}}{2cn_2}A_1^2e^{i\Delta k_0 Z}\\
&\quad+\frac{\pi 3\omega_2\chi^{(3)}}{2cn_2}\left(|A_2|^2+2|A_1|^2\right)A_2=0.
\end{aligned} \tag{2}$$

where $T=t-Z/V_g$ with $V_g=1/(\partial k_{1,2}/\partial\omega_{1,2})$ being the group velocities, $K=(\partial^2 k_{1,2}/\partial\omega_{1,2}^2)$ are the group-velocity dispersion (GVD) parameters. In the context of this study, we assume that the Poynting-vector walkoff between FF and SH modes is negligible [61–68]. It should be noted that there is a limit on the minimal temporal size of a pulse to admit vortices [69]. Thus, one has $V_g=V_{g1}=V_{g2}=1/(\partial k_{1,2}/\partial\omega_{1,2})$, $K=K_1=K_2=(\partial^2 k_{1,2}/\partial\omega_{1,2}^2)$. $\Delta k_0=2k_1-k_2$ is the phase mismatch. $n_{1,2}$ are the refractive indices of FF and SH modes in the QPM photonic crystal; $\chi^{(2)}$ and $\chi^{(3)}$ are the second- and third-order susceptibilities.

Here, the 3D periodically modulated $\chi^{(2)}$ susceptibility is determined by a checkerboard setup constructed as $\chi^{(2)}=\sigma(X,Y)d(Z)$, where $\sigma(X,Y)=-\text{sgn}\{\cos(\pi X/D)\cos(\pi Y/D)\}$ and $d(Z)=d_0\text{sgn}\cos(2\pi Z/\Lambda)$ with d_0 being the coefficient of modulation in the Z direction, $D\times D$ represents the size of checkerboard cell, and Λ is the modulation period with duty cycle 1/2 [70], as shown in Figs. 1(a), (b) and (c). In the direction of propagation along the Z-axis, the function $d(Z)$ can be formulated via a Fourier expansion due to their dominant role in QPM, wherein only the fundamental harmonic terms remain, while the influence of higher-order harmonics is negligible [52].

By introducing the rescaled coordinates, Eq. (2) can be normalized to a non-dimensional nonlinear Schrödinger equation (NLSE)

$$\begin{aligned}
i\frac{\partial\psi_1}{\partial z}=&-\frac{1}{2}\left(\frac{\partial^2\psi_1}{\partial x^2}+\frac{\partial^2\psi_1}{\partial y^2}\right)-\frac{\rho}{2}\frac{\partial^2\psi_1}{\partial\tau^2}-\Omega\psi_1\\
&-2\sigma(x,y)\psi_1^*\psi_2+\left(g_{11}|\psi_1|^2+g_{12}|\psi_2|^2\right)\psi_1\\
i\frac{\partial\psi_2}{\partial z}=&-\frac{1}{4}\left(\frac{\partial^2\psi_2}{\partial x^2}+\frac{\partial^2\psi_2}{\partial y^2}\right)-\frac{\rho}{4}\frac{\partial^2\psi_2}{\partial\tau^2}-\Omega\psi_2\\
&-\sigma(x,y)\psi_1^2+\left(g_{22}|\psi_2|^2+g_{12}|\psi_1|^2\right)\psi_2,
\end{aligned} \tag{3}$$

Here, the transverse and longitudinal coordinates are rescaled as $(x,y)=(X,Y)\sqrt{k_1/z_d}$ and $z=Z/z_d$ with $z_d^{-1}=\frac{2}{c\pi}\frac{d_0^2}{\chi^{(3)}}\sqrt{\left(\frac{\omega_1^2\omega_2}{n_1^2n_2}\xi\right)}$, $\xi=\left(n_1/\omega_1+n_2/\omega_2\right)$ [71]. The time is rescaled as $\tau=T/T_0$ where T_0 is the typical pulse duration. The symbol $\rho=-Kz_d/T_0^2$ represents the ratio of different GVD coefficients at the two harmonics [66,67], where an anomalous dispersion with $K<0$ is adopted. In this work, we take $\rho=1$ for simplicity. The wavefunctions of FF and SH modes are rescaled as $\psi_{1,2}=\frac{\chi^{(3)}}{d_0}\sqrt{\frac{n_{1,2}}{\omega_{1,2}\xi}}A_{1,2}\exp\left[i\left(\Delta k_0-2\pi/\Lambda\right)Z\right]$. $\Omega=z_d(\Delta k_0-2\pi/\Lambda)$ in the right side of Eq. (4) is the mismatch. Previous research has proven that the states of vortex solitons are most stable with the perfect phase matching condition, leading to $\Omega=0$ [52] which is taken in this work.

In this work, $\chi^{(3)}$ is supposed to be tunable as $\chi^{(3)}=\eta\chi_0^{(3)}$, where $\chi_0^{(3)}$ is the fundamental value that related to the intrinsic characteristics of media, and η represents the shift from the fundamental value. The strength coefficients for the cubic nonlinearity are $g_{11}=\frac{3\pi\eta}{4}\sqrt{\frac{\omega_1^2n_2}{n_1^2\omega_2}}\xi$, $g_{12}=\frac{3\pi\eta}{2}\sqrt{\frac{\omega_2}{n_2}}\xi$, and $g_{22}=\frac{3\pi\eta}{4}\sqrt{\frac{\omega_2^3n_1^2}{n_2^3\omega_1^2}}\xi$. The difference of the refractive indices for the FF and SH modes is supposed to be negligible, i.e., $n_1\approx n_2$. Then, the cubic nonlinear coefficients are $g_{11}=3\pi\eta\sqrt{3}/8$, $g_{12}=g_{22}=4g_{11}$ [71]. Under the above approximation, the non-dimensional NLSE (3) can be expressed as

$$\begin{aligned}
i\frac{\partial\psi_1}{\partial z}&=-\frac{1}{2}\nabla_{x,y,\tau}^2\psi_1-2\sigma(x,y)\psi_1^*\psi_2+g_{11}\left(|\psi_1|^2+4|\psi_2|^2\right)\psi_1,\\
i\frac{\partial\psi_2}{\partial z}&=-\frac{1}{4}\nabla_{x,y,\tau}^2\psi_2-\sigma(x,y)\psi_1^2+4g_{11}\left(|\psi_2|^2+|\psi_1|^2\right)\psi_2,
\end{aligned} \tag{4}$$

where $\nabla_{x,y,\tau}^2=\left(\partial^2/\partial x^2+\partial^2/\partial y^2+\partial^2/\partial\tau^2\right)$.

A longitudinal twist with rotating frequency α is performed on the photonic crystal, then the new coordinates (x',y',z') in the rotational system satisfy the following relation:

$$\begin{aligned}
x'(z)&=x\cos(\alpha z)-y\sin(\alpha z),\\
y'(z)&=x\sin(\alpha z)+y\cos(\alpha z),\\
z'&=z.
\end{aligned} \tag{5}$$

Here, the rotation scheme can be described as involving a screw-based fabrication approach through the QPM [72,73], and have been theoretically explored [74,75] and realized in experiment [76,77]. By substituting Eq. (5) into Eq. (4), one can obtain the following coupled

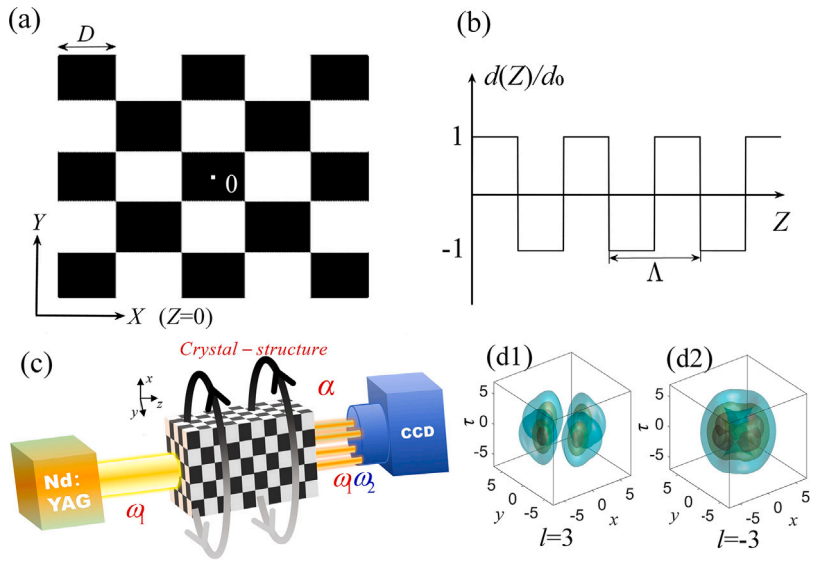

Fig. 1. (a) Checkerboard structure of the nonlinear lattice. White and black cells correspond to $\sigma(x, y) = +1$ and -1, respectively. (b) Modulation along the propagation distance with period Λ. (c) Schematic of the experimental setup. (d) Eigenstates $|\psi_{1,2}|$ of vortex LBs with topological charge $l = 3$ (d1) and $l = -3$ (d2). Here only rhombus-typed LBs with FF mode are plotted, and the system parameters are $P = 100$, $D = 3$, $\alpha = 0.2$, $g_{11} = 0.1$.

NLSE:

$$\begin{aligned} i\frac{\partial\psi_1}{\partial z} &= -\frac{1}{2}\nabla^2_{x,y,\tau}\psi_1 - 2\sigma(x,y)\psi_1^*\psi_2 \\ &\quad + g_{11}\left(|\psi_1|^2 + 4|\psi_2|^2\right)\psi_1, + i\alpha\left(x\frac{\partial\psi_1}{\partial y} - y\frac{\partial\psi_1}{\partial x}\right), \\ i\frac{\partial\psi_2}{\partial z} &= -\frac{1}{4}\nabla^2_{x,y,\tau}\psi_2 - \sigma(x,y)\psi_1^2 \\ &\quad + 4g_{11}\left(|\psi_2|^2 + |\psi_1|^2\right)\psi_2 + i\alpha\left(x\frac{\partial\psi_2}{\partial y} - y\frac{\partial\psi_2}{\partial x}\right). \end{aligned} \tag{6}$$

The primes in the coordinates x', y', and z' in Eq. (6) are omitted.

The total Hamiltonian of this system is defined as

$$H = \int\int\int \left(H_P + H_{\chi^{(2)}} + H_{\chi^{(3)}} + H_\alpha\right) \mathrm{d}x\mathrm{d}y\mathrm{d}\tau \tag{7}$$

where $H_P = \frac{1}{2}\left|\nabla_{x,y,\tau}\psi_1\right|^2 + \frac{1}{4}\left|\nabla_{x,y,\tau}\psi_2\right|^2$, $H_{\chi^{(2)}} = -\sigma(x,y)[(\psi_1^*)^2\psi_2 + \mathrm{c.c.}]$, $H_{\chi^{(3)}} = \frac{1}{2}g_{11}|\psi_1|^4 + g_{12}|\psi_1|^2|\psi_2|^2 + \frac{1}{2}g_{22}|\psi_2|^4$, and $H_\alpha = \frac{i}{2}\alpha\left[\psi_1^*\left(x\frac{\partial\psi_1}{\partial y} - y\frac{\partial\psi_1}{\partial x}\right) + \psi_2^*\left(x\frac{\partial\psi_2}{\partial y} - y\frac{\partial\psi_2}{\partial x}\right) + \mathrm{c.c.}\right]$ with c.c. representing the complex conjugate.

The power of LBs (alias the Manley–Rowe invariant [78,79]) is defined as $P = \int\int\int \left(|\psi_1|^2 + 2|\psi_2|^2\right)\mathrm{d}x\mathrm{d}y\mathrm{d}\tau = P_1 + P_2$, where P_1 and P_2 correspond to the power of FF and SH components, respectively. The power ratio $\gamma = P_2/P_1$ is defined to evaluate the power conversion from FF to SH modes.

3. Results and discussions

To obtain stable solution of Eq. (6), the wavefunctions of light fields are expressed in the form $\psi_{1,2} = \phi_{1,2}e^{i\beta_{1,2}z}$, where the indices 1 and 2 represent the FF and SH modes, $\phi_{1,2}$ are stationary solutions that are independent of the propagation distance z, and $\beta_{1,2}$ are propagation constants that satisfy the relation $\beta_2 = 2\beta_1 = 2\beta$. The initial input beams are taken in the following form:

$$\phi_j = \left(\frac{\sqrt{2x^2+2y^2+2\tau^2}}{w_0}\right)^{|l_j|} e^{-\frac{(x-x_0)^2+(y-y_0)^2+(\tau-\tau_0)^2}{w_0^2}} L_{p_j}^{|l_j|}\left[\frac{2x^2+2y^2+2\tau^2}{w_0^2}\right] e^{il_j\theta}, \tag{8}$$

where $j = 1, 2$, w_0 is the width of laser field, $L_{p_j}^{|l_j|}$ are the generalized Laguerre–Gauss polynomials, θ is the azimuthal angle, l and p are radial and azimuthal indices, respectively. In this work, l can be taken as an integer topological charge.

By substituting $\psi_{1,2}$ into Eq. (6), and performing the accelerated imaginary-time evolution methods [80], the stationary solution (eigenstates $\psi_{1,2}$) can be obtained numerically. The matching conditions are $\varphi_2 = 2\varphi_1 - \varphi_d$ or $\varphi_d = 2\varphi_1 - \varphi_2$, where $\varphi_{1,2} = \mathrm{Arg}\{\phi_{1,2}\}$ and φ_d are determined by $\sigma(x, y)$. We get $\varphi_d = 0$ and π with $\sigma(x, y) = +1$ and -1, respectively. Under the condition $p = 0$, rhombus- and square-shaped vortex LBs, corresponding to $\varphi_d = 0$ and π, are found. Each shaped vortex LBs has two components, FF and SH modes. The rotational system can support vortex LBs with $l = 1 \sim 3$. Examples of rhombus-shaped vortex LBs with $l = +3$ and $l = -3$ are shown in Figs. 1(d1) and (d2), respectively. In this paper, the LB profiles are plotted with moduli of eigenstates $|\psi_{1,2}|$. The vortex LBs can be considered as stable when their profiles do not undergo significant changes over a propagation distance of $z = 500$. In comparison, non-rotating QPM systems with pure quadratic nonlinearity can only support vortex solitons with topological charge of 1 [52]. On the other hand, vortices with high topological charges can be obtained in two-dimensional bulk systems with competing cubic–quintic nonlinearities [81]. In the context of this paper, vortices of higher topological charges are achieved due to the rotation of system and the competing quadratic–cubic nonlinearity [82].

The 3D profiles of vortex LBs and their projections/phases in (x, y) plane under varying cubic nonlinear coefficient g_{11} are illustrated in Fig. 2. The rhombus- and square-shaped vortex LBs are shown in the first and second rows, respectively. Only the FF mode is given as the cases for SH mode are similar to FF mode. A notable elongation of 3D vortex LBs along the τ-axis becomes evident with the modulation of cubic nonlinearity g_{11}, indicating a distortion in the LBs' shape which is perpendicular to the transverse plane. The projections of vortex LBs in the (x, y) plane remain relatively unchanged. Specifically, the phase structure distributions present a vortex pattern, corresponding to a topological charge of $l = 1$.

Fig. 3 focuses on the detailed iso-surface of rhombus- and square-shaped vortex LBs with varying rotating frequency α. Under non-rotating conditions ($\alpha = 0$), both rhombus- and square-shaped vortex LBs exhibit a clear four-peak pattern, reflecting the geometry of a checkerboard lattice. The two kinds of vortex LBs are localized at the white and black cells of the checkerboard lattice, respectively. The

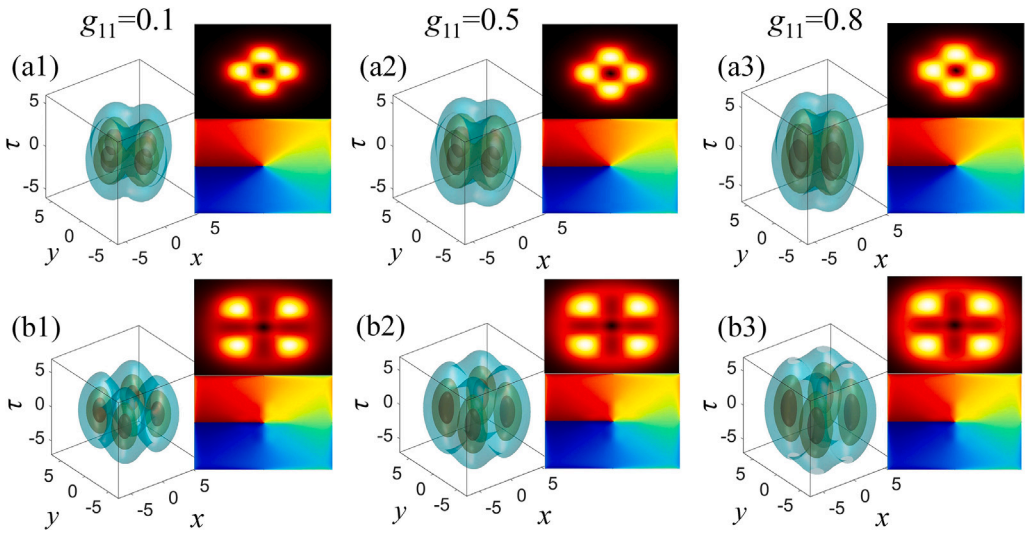

Fig. 2. Vortex LBs with various $g_{11} = 0.1, 0.5, 0.8$. The 3D profiles of vortex LBs are plotted with moduli of eigenstates $|\psi_{1,2}|$, projections and phases in the (x, y) plane. The first and second rows are the cases for rhombus- and square-shaped vortex LBs. System parameters are $(\alpha, P, D, l, p) = (0.2, 60, 3, 1, 0)$.

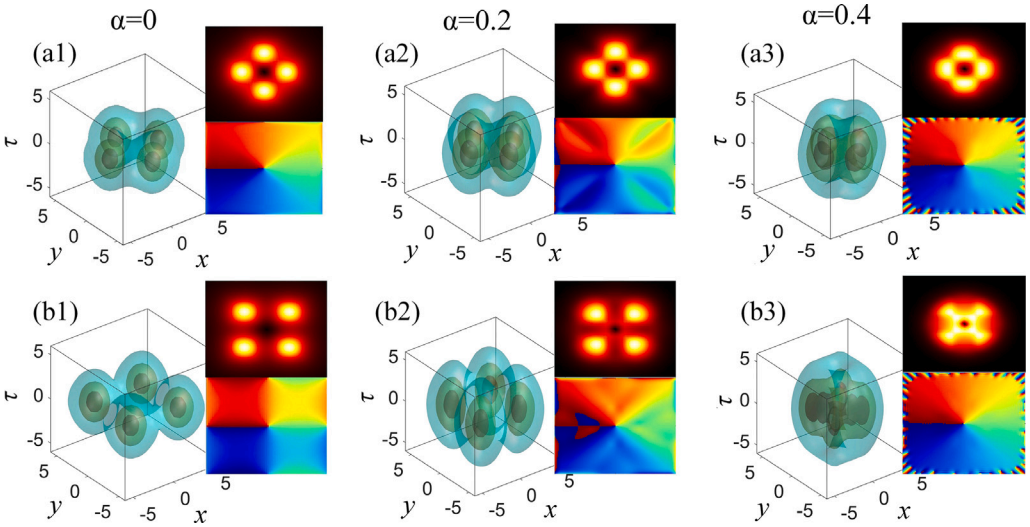

Fig. 3. Vortex LBs with various $\alpha = 0, 0.2, 0.4$. The first and second rows are the cases for rhombus- and square-shaped vortex LBs. System parameters are $(g_{11}, P, D, l, p) = (0.1, 60, 3, 1, 0)$.

distinct separation between these peaks indicates a well-defined spatial localization. However, the boundaries separating the peaks become increasingly blurred with the increase of α. Furthermore, the distance between the peaks decreases, indicating that the peaks are moving closer together. These changes reflect a reconfiguration of the intensity landscape of vortex LBs in response to rotational dynamics. Additionally, the phase of vortex LBs undergoes a transition from a quadrupole pattern to the typical vortex mode with increasing α [53], where the phase presents a continuous and smooth manner.

This rotational system can support vortex LBs with topological charges up to $l = 3$, as shown in Fig. 4. Here the rotating frequency is taken as $\alpha = 0.2$, and the cubic nonlinearity coefficient is $g_{11} = 0.1$. Rhombus-shaped vortex LBs with FF and SH modes are shown here. It is found that the profiles of vortex LBs in the (x, y) plane expand with increasing topological charges, while the profiles in the τ direction remain unchanged. In the azimuthal direction, the phase structures present periodical gradient changes which are determined by topological charge l. For the FF mode, the phase periodical cycle equals to l, while it is twice the value of l for SH mode.

According to Figs. 2–4, we observe that the sizes of vortex LBs present different responses to the modulation of parameters g_{11}, α and l. Here, the width of vortex LBs with FF mode in (x, y) plane is defined as $W_{\mathrm{FF}} = \sqrt{\int\int\int x^2|\psi_1|^2 \mathrm{d}x\mathrm{d}y\mathrm{d}\tau / \int\int\int |\psi_1|^2 \mathrm{d}x\mathrm{d}y\mathrm{d}\tau}$. We have conducted a thorough investigation and presented the relationship between the width and control parameters in Fig. 5. The results indicate that the width of vortex LBs increases with topological charge l, whereas it monotonically decreases with both α and g_{11}.

The Hamiltonian H, propagation constant β, and power ratio γ as functions of control parameters α, P, D, and g_{11} are demonstrated in Fig. 6. It is found that the rhombus-shaped vortex LBs exhibit a lower Hamiltonian compared to the square-shaped ones, as shown in Figs. 6(a1, b1, c1, d1). This phenomenon stems from the tightly bounding ground state of rhombus-shaped vortex. The $\beta(P)$ curve in Fig. 6(b2)

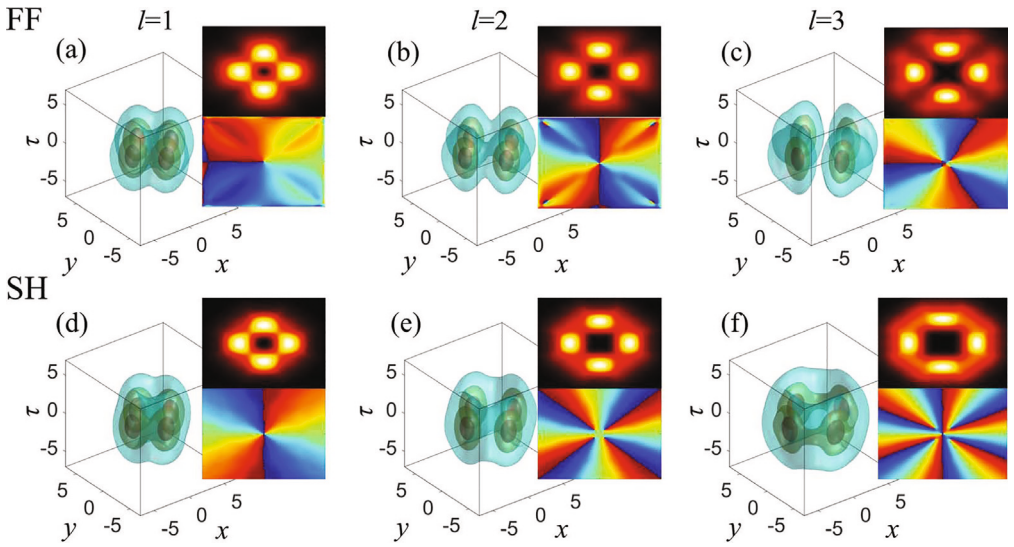

Fig. 4. Vortex LBs with various topological charges $l = 1, 2, 3$. The rhombus-shaped vortex LBs are taken for example. The first and second rows are LBs with FF and SH modes, respectively. System parameters are $(\alpha, g_{11}, P, D, l, p) = (0.2, 0.1, 80, 3, 1, 0)$.

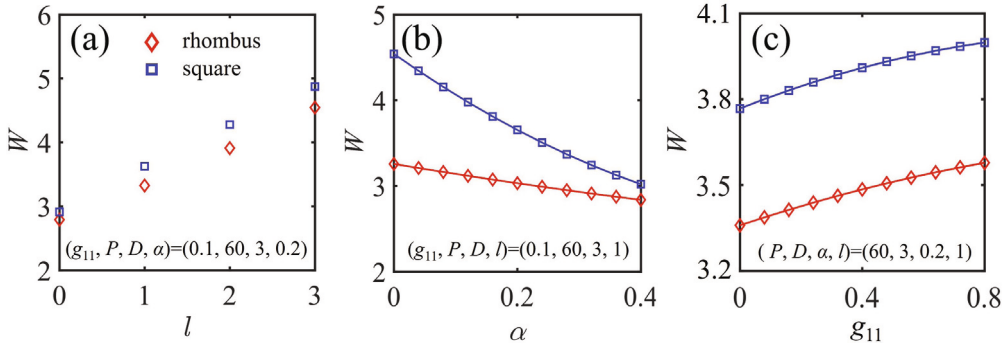

Fig. 5. Width of vortex LBs vs l (a), α (b), and g_{11} (c). The other parameters are $l = 1$, $p = 0$.

has the relation $dP/d\beta < 0$, satisfying the Vakhitov–Kolokolov (VK) criterion which is typically associated with the stability of solitons with self-focusing nonlinearity [83]. Further, the power ratio $\gamma = P_2/P_1$ decreases monotonically with α [Fig. 6(a3)]. On the other hand, γ would increase with P [Fig. 6(b3)], indicating that the conversion efficiency from FF to SH might improve at higher power levels. Another finding is that the power ratio γ remains unaffected by changing the cell size D [Fig. 6(c3)], agreeing with the previous research on 2D QPM photonic crystal [52]. Furthermore, there is only a slight increase in the power ratio γ when there is an increase in cubic nonlinear coefficient g_{11} [Fig. 6(d3)].

The stability domains of this system in the (α, g_{11}), (D, g_{11}), and (P, g_{11}) planes are depicted in Fig. 7. Here, only the vortex LBs with topological charge $l = 1$ are presented. The stability domains for rhombus- and square-shaped vortex LBs are indicated by red and blue areas, respectively. The overlapping areas of these two types are shown in purple. It is found that the rhombus-shaped vortex LBs exhibit a larger stability region compared to their square-shaped counterpart. There are considerable overlapping areas for the two types of LBs. In the (α, g_{11}) plane, the stability regions of rhombus- and square-shaped vortex LBs are almost overlapping [Fig. 7(a)]. While the stability regions of square-shaped vortex LBs are completely covered by that of rhombus-shaped ones in the (D, g_{11}) plane [Fig. 7(b)]. The stability domain in the (P, g_{11}) plane exhibits a non-monotonic trend, first increasing and then decreasing with the increasing of g_{11} [Fig. 7(c)]. These results demonstrate that g_{11} plays a key role in the stability domains of vortex LBs, and rhombus-shaped vortex LBs exhibit larger stability domains than square-shaped ones, agreeing with the conclusions drawn from Fig. 6(a1,b1,c1,d1).

Another characteristic of the vortex LBs is the orbital angular momentum (OAM) in the (x, y) plane, which is defined as

$$\langle L_{1,2} \rangle = \int \frac{\left(\psi_{1,2}^* \hat{L} \psi_{1,2} + \text{c.c.}\right)}{2P_{1,2}} \mathrm{d}x\mathrm{d}y,$$
$$\langle L \rangle = \frac{P_1 \langle L_1 \rangle + P_2 \langle L_2 \rangle}{P}, \tag{9}$$

where c.c. stands for complex conjugate, $L_{1,2}$ and L represent the OAM of the FF/ SH components and total one, respectively; $\hat{L} = -i(x\partial/\partial y - y\partial/\partial x)$ is the OAM operator. Fig. 8 depicts the OAM of vortex LBs as functions of control parameters α, g_{11}, and l. For a non-rotational system $\alpha = 0$, the values of OAM are proportional to topological charges [84]. Under the influence of rotation and cubic nonlinearities, some derivations of OAM can be observed. By modulating α and g_{11}, it is found that the total OAM monotonically increases with α, while it decreases with g_{11}. The reason is that an artificial angular momentum is introduced by rotating frequency α, the total OAM of the system can be regarded as the superposition of this artificial angular momentum and the intrinsic angular momentum derived from the topological charge.

A significant finding of this paper is that the rotating QPM system can support vortex LBs with topological charges up to $l = 3$. In contrast, only vortex solitons with $l = 1$ can be achieved in a 2D non-rotating QPM system [52]. To test the stability of these vortex LBs with higher

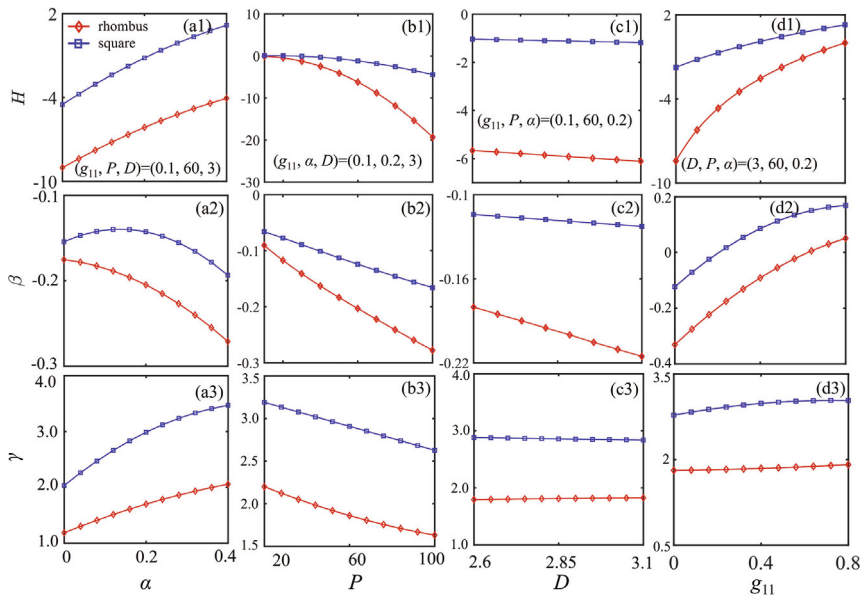

Fig. 6. Modulation of Hamiltonian H, propagation constant β, and power ratio γ as functions of control parameters α, P, D, and g_{11}. The topological charge is taken as $l = 1$. The fixed parameters are shown in the first panel of each column.

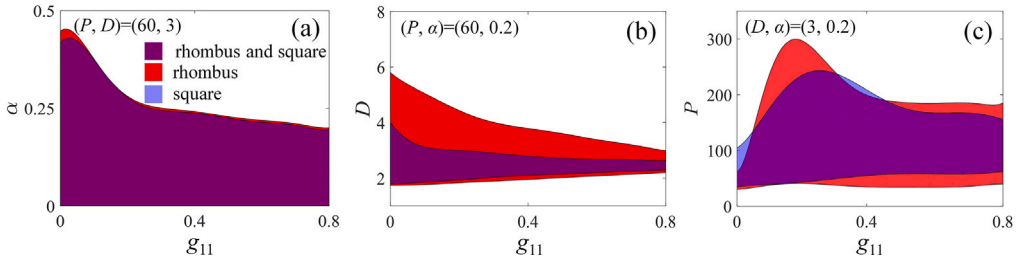

Fig. 7. Stability domains in the (α, g_{11}), (D, g_{11}), and (P, g_{11}) planes. The red and blue areas represent the stability domains of rhombus and square-shaped vortex LBs, respectively. The purple area is the overlapping region for both two types. The stability domains are identified using vortex LBs that can propagate over distances greater than $z = 500$.

topological charges, we conducted direct simulations of Eq. (6) using the fourth-order Runge–Kutta method. The evolution of vortex LBs with $l = 3$ is plotted in Fig. 9, where the 3D eigenstates $|\psi_1|$, their projections and phase structures in (x, y) plane are shown. Firstly, it is observed that during the propagation along z direction, the four peaks of vortex LBs rotate counterclockwise around the center of (x, y) plane, which is attributed to the coordinate rotation. Secondly, the temporal and spatial localization of the vortex LBs remains largely robust. Lastly, vortex LBs with $l = 3$ can propagate stably up $z = 800$. Further investigations have shown that LBs with lower topological charges can propagate longer. One example of vortex LBs with $l = 1$ is shown in Fig. 10.

It is noticed that the radius of the Laguerre-Gaussian beam in Eq. (8) can be modulated by parameters l and p, as shown in Fig. 11. The rhombus- and square-shaped vortex LBs are obtained with $(l, p) = (1, 0)$, as shown in Figs. 11(a) and (b). It can be observed that 8 blocks, including 4 white and 4 black blocks, are covered by the input light beam. The white and black blocks indicate $\sigma = +1$ and -1, corresponding to $\varphi_d = 0$ and π, respectively. When the initial beams of FF and SH modes satisfy the matching condition $\varphi_d = 0$, the rhombus-shaped vortex LBs would be generated in the four white blocks, as shown in Fig. 11(a). On the other hand, with matching condition $\varphi_d = \pi$, the square-shaped vortex LBs would be generated in the four black blocks, as shown in Fig. 11(b). With suitable values of l and p, one can get more complex shaped vortex LBs. For example, two kinds of necklace vortex LBs with eight peaks would be obtained when $(l, p) = (1, 4)$, as shown in Figs. 11(c) and (d), where they are generated in white and black blocks, respectively. The stability of these 8-core necklace vortex LBs is confirmed by the propagation evolution, as shown in Fig. 12.

To assess the propagation distance of vortex LBs in experiment, we adopt Lithium niobate as a potential candidate where the refractive indices $n_1 \approx n_2 = 2.2$, quadratic nonlinearity coefficient $d_0 = 2.1\,\mathrm{pm/V}$ [85], and the cubic nonlinearity coefficient $\chi_0^{(3)} = 6.6 \times 10^{-22}\,\mathrm{m^2/V^2}$ [86]. The wavelengths of FF and SH modes are chosen as 1064 nm and 532 nm, respectively, with an electric field amplitude $A_0 = 200\,\mathrm{kV/cm}$ and pulse duration $T_0 = 100\,\mathrm{ps}$ [87]. The propagation distance scale is estimated as $z_d = 0.05\,\mathrm{mm}$. Thus, the physical propagation distance $z = 800$ is about 40 mm for vortex LBs with topological charge $l = 3$ in the simulation, which is enough for the observation in the experiment.

4. Conclusions

In conclusion, our study presents a novel approach for generating and manipulating stable vortex LBs within a rotating QPM photonic crystal characterized by its unique rotational checkerboard structure. This setup considers the interplay between competing quadratic and cubic nonlinearities, enabling the observation of three distinct vortex LB configurations: square-, rhombus-, and necklace-shaped patterns.

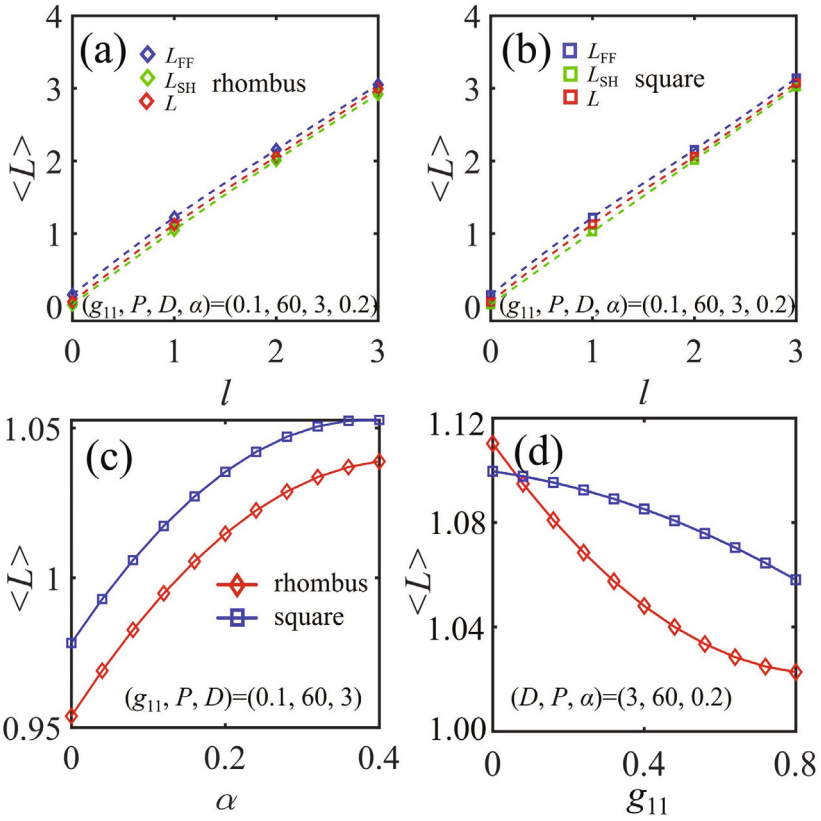

Fig. 8. Angular momentum vs l (a, b), α (c), and g_{11} (d). Panels (a) and (b) are OAM for rhombus- and square-shaped vortex LBs, respectively.

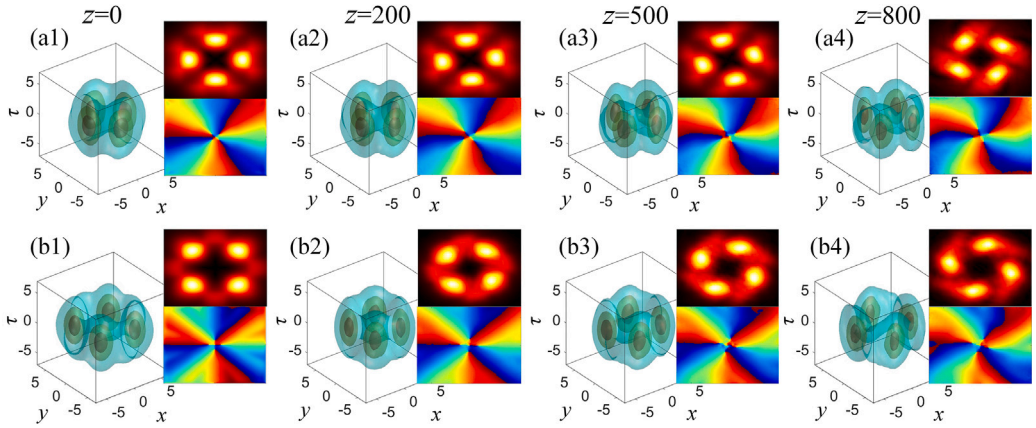

Fig. 9. Propagation of vortex LBs, where the propagation distances are taken as $z = 0, 200, 500, 800$. In each panel, the 3D eigenstates $|\psi_1|$, their projections and phase structures in (x, y) plane are shown. The FF mode for rhombus- and square-shaped vortex LBs are shown. The topological charge is taken $l = 3$ for example. The other parameters are $(\alpha, g_{11}, P, D) = (0.2, 0.1, 100, 3)$.

The versatility of this system lies in its ability to dynamically control the vortex LBs through system parameters, such as input power, rotating frequency, checkerboard cell size, and azimuthal indices of the incident light.

Our findings demonstrate that the vortex LBs in this competing quadratic–cubic nonlinearity can support higher topological charges comparing stable 2D vortex solitons observed in pure quadratic systems. Owing to the artificial angular momentum induced by rotation, the total OAM can be strengthened or weakened, leading to a new balance of vortex LBs with high topological charges. This enhanced capability is particularly noteworthy, as it opens up avenues for generating more complex and powerful vortex structures with potential applications in advanced optical technologies. Furthermore, the rotating frequency triggers a fascinating transition from quadrupole vortex LBs to typical vortex modes, highlighting the rich dynamics achievable within this system. It should be noted that we mainly concentrate on the defocusing cubic term. The reason lies in the competing quadratic–cubic nonlinearity. Generally, in order to achieve the balance between the quadratic and cubic nonlinearities, the signs of the two coefficients should be the opposite. Thus, in this work, we mainly consider the defocusing cubic nonlinearity $g_{11} > 0$ and focusing quadratic nonlinearity. In the simulations, we also tried the focusing case $g_{11} < 0$, however, we could not obtain any stationary solutions.

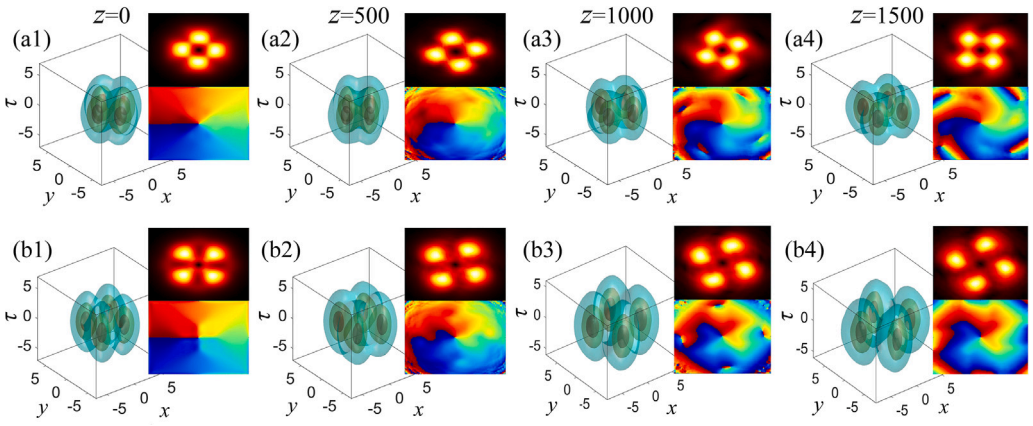

Fig. 10. Propagation of vortex LBs, where the propagation distances are $z = 0, 500, 1000, 1500$. The topological charge is taken $l = 1$ for example. The other parameters are $(\alpha, g_{11}, P, D) = (0.2, 0.1, 100, 3)$.

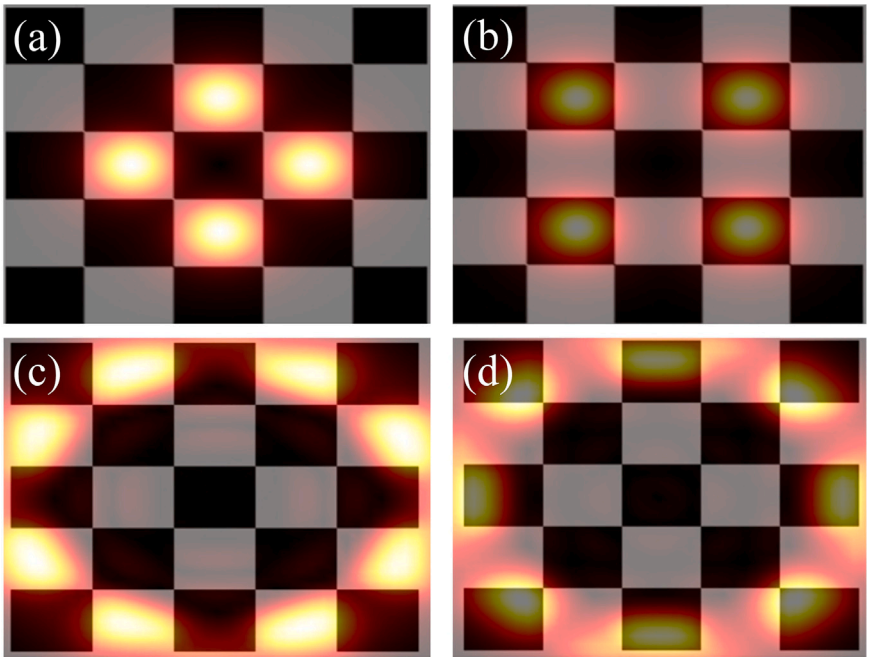

Fig. 11. Geometry of Laguerre-Gaussian beam and checkerboard lattice. (a, b) Rhombus- and square-shaped vortex LBs are located in white and black blocks, respectively. The parameters are $(l, p) = (1, 0)$. (c, d) Eight-core necklace vortex LBs are located in white and black blocks, respectively. The parameters are $(l, p) = (1, 4)$.

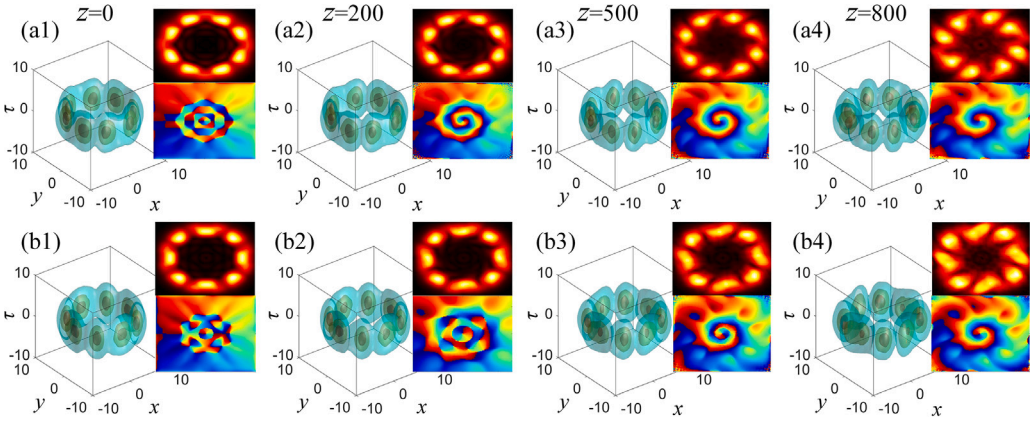

Fig. 12. Vortex LBs with big radius and their propagation. The parameters are the same as Fig. 11.

CRediT authorship contribution statement

Shunfang Chen: Supervision, Conceptualization. **Linjia Wang:** Software, Investigation. **Zhuo Fan:** Formal analysis. **Wei Peng:** Data curation. **Di Wu:** Writing – original draft. **Yuan Zhao:** Writing – original draft, Methodology. **Siliu Xu:** Writing – review & editing, Funding acquisition.

Declaration of competing interest

The authors declare that they have no known competing financial interests or personal relationships that could have appeared to influence the work reported in this paper.

Acknowledgments

This work was supported by the National Natural Science Foundation of China (62275075), Science and technology research program of the Education Department of Hubei Province, China (B2022188), Medical Project of Hubei University of Science and Technology, China (2023YKY08), Natural Science Foundation of Hubei Province, China (2023AFC042), and Training Program of Innovation and Entrepreneurship for Undergraduates of Hubei Province, China (S202210927003).

Data availability

Data will be made available on request.

References

[1] Silberberg Y. Collapse of optical pulses. Opt Lett 1990;15:1282–4.
[2] Chen Y, Atai J. Dark optical bullets in light self-trapping. Opt Lett 1995;20:133.
[3] Firth WJ, Scroggie AJ. Optical bullet holes: robust controllable localized states of a nonlinear cavity. Phys Rev Lett 1996;76:1623.
[4] Malomed BA, Mihalache D, Wise F, Torner L. Spatiotemporal optical solitons. J Opt B 2005;7:R53.
[5] Akhmediev N, Soto-Crespo JM. Generation of a train of three-dimensional optical solitons in a self-focusing medium. Phys Rev A 1993;47:1358.
[6] Mihalache D, Mazilu D, Lederer F, Kivshar YS. Collisions between discrete surface spatiotemporal solitons in nonlinear waveguide arrays. Phys Rev A 2009;79:013811.
[7] Edmundson DE, Enns RH. Fully 3-dimensional collisions of bistable light bullets. Opt Lett 1993;18:1609.
[8] Edmundson DE, Enns RH. The particle-like nature of colliding light bullets. Phys Rev A 1995;51:2491.
[9] Kivshar YS, Agrawal GP. Optical solitons: from fibers to photonic crystals. San Diego, CA, USA: Academic Press; 2003.
[10] Li G, Zhao Z, Jiang X, Chen Z, Liu B, Malomed BA, Li Y. Strongly anisotropic vortices in dipolar quantum droplets. Phys Rev Lett 2024;133:053804.
[11] Zhang X, Xu X, Zheng Y, Chen Z, Liu B, Huang C, Malomed BA, Li Y. Semidiscrete quantum droplets and vortices. Phys Rev Lett 2019;123:133901.
[12] Weinstein MI. Nonlinear Schrödinger equations and sharp interpolation estimates. Comm Math Phys 1983;87:567.
[13] Bergé L. Wave collapse in physics: principles and applications to light and plasma waves. Phys Rep 1998;303:259.
[14] Fibich G, Papanicolaou G. Self-focusing in the perturbed and unperturbed nonlinear Schrödinger equation in critical dimension. SIAM J Appl Math 1999;60:183.
[15] Sulem C, Sulem P-L. The nonlinear Schrödinger equation: self-focusing and wave collapse. New York: Springer; 1999.
[16] Kuznetsov EA, Dias F. Bifurcations of solitons and their stability. Phys Rep 2011;507:43.
[17] Zakharov VE, Kuznetsov EA. Solitons and collapses: two evolution scenarios of nonlinear wave systems. Phys-Usp 2012;55:535.
[18] Mihalache D. Multidimensional localized structures in optics and Bose–Einstein condensates: A selection of recent studies. Romanian J Phys 2014;59:295.
[19] Malomed BA. Multidimensional solitons: Well-established results and novel findings. Eur Phys J Spec Top 2016;225:2507.
[20] Liao B, Li S, Huang C, Luo Z, Pang W, Tan H, Malomed BA, Li Y. Anisotropic semivortices in dipolar spinor condensates controlled by Zeeman splitting. Phys Rev A 2017;96:043613.
[21] Mihalache D, Mazilu D, Lederer F, Kartashov YV, Crasovan L-C, Torner L, Malomed BA. Stable vortex tori in the three-dimensional cubic-quintic Ginzburg–Landau equation. Phys Rev Lett 2006;97:073904.
[22] Liu X, Qian L-J, Wise FW. Generation of optical spatiotemporal solitons. Phys Rev Lett 1999;82:4631.
[23] Minardi S, Eilenberger F, Kartashov YV, Szameit A, Röpke U, Kobelke J, et al. Three-dimensional light bullets in arrays of waveguides. Phys Rev Lett 2010;105:263901.
[24] Eilenberger F, Prater K, Minardi S, Geiss R, Röpke U, Kobelke J, et al. Observation of discrete vortex light bullets. Phys Rev X 2013;3:041031.
[25] Lahav O, Kfir O, Sidorenko P, Mutzafi M, Fleischer A, Cohen O. Three-dimensional spatiotemporal pulse-train solitons. Phys Rev X 2017;7:041051.
[26] Kartashov YV, Malomed BA, Torner L. Solitons in nonlinear lattices. Rev Modern Phys 2011;83:247.
[27] Torner L, Kartashov YV. Light bullets in optical tandems. Opt Lett 2009;34:1129.
[28] Song L, Yang Z, Li X, Zhang S. Controllable Gaussian-shaped soliton clusters in strongly nonlocal media. Opt Express 2018;26:19182.
[29] Reyna AS, Boudebs G, Malomed BA, de Araújo CB. Robust self-trapping of vortex beams in a saturable optical medium. Phys Rev A 2016;93:013840.
[30] Burgess IB, Peccianti M, Assanto G, Morandotti R. Accessible light bullets via synergetic nonlinearities. Phys Rev Lett 2009;102:203903.
[31] Peccianti M, Burgess IB, Assanto G, Morandotti R. Space–time bullet trains via modulation instability and nonlocal solitons. Opt Express 2010;18:5934.
[32] Mihalache D, Mazilu D, Malomed BA, Lederer F, Crasovan L-C, Kartashov YV, Torner L. Stable three-dimensional optical solitons supported by competing quadratic and self-focusing cubic nonlinearities. Phys Rev E 2006;74:047601.
[33] Mihalache D, Mazilu D, Crasovan LC, Towers I, Malomed BA, Buryak AV, Lederer F. Stable three-dimensional spinning optical solitons supported by competing quadratic and cubic nonlinearities. Phys Rev E 2002;66:016613.
[34] Mihalache D, Mazilu D, Crasovan L-C, Torner L, Malomed BA, Lederer F. Three-dimensional walking spatiotemporal solitons in quadratic media. Phys Rev E 2000;62:7340.
[35] Yang J, Musslimani ZH. Fundamental and vortex solitons in a two-dimensional optical lattice. Opt Lett 2003;28:2094.
[36] Rodas-Verde MI, Michinel H, Kivshar YS. Dynamics of vector solitons and vortices in two-dimensional photonic lattices. Opt Lett 2006;31:607–9.
[37] Aceves AB, De Angelis C, Rubenchik AM, Turitsyn SK. Multidimensional solitons in fiber arrays. Opt Lett 1994;19:329.
[38] Aceves AB, Luther GG, De Angelis C, Rubenchik AM, Turitsyn SK. Energy localization in nonlinear fiber arrays: collapse-effect compressor. Phys Rev Lett 1995;75:73.
[39] Mihalache D, Mazilu D, Lederer F, Kartashov YV, Crasovan L-C, Torner L. Stable three-dimensional spatio-temporal solitons in a two-dimensional photonic lattice. Phys Rev E 2004;70:055603(R).
[40] Mihalache D, Mazilu D, Lederer F, Malomed BA, Kartashov YV, Crasovan LC, et al. Stable Spatiotemporal solitons in Bessel optical lattices. Phys Rev Lett 2005;95:023902.
[41] Leblond H, Malomed BA, Mihalache D. Three-dimensional vortex solitons in quasi two-dimensional lattices. Phys Rev E 2007;76:026604.
[42] Leblond H, Malomed BA, Mihalache D. Spatio-temporal vortex solitons in hexagonal arrays of waveguides. Phys Rev A 2011;83:063825.
[43] Cheskis D, Bar-Ad S, Morandotti R, Aitchison JS, Eisenberg HS, Silberberg Y, et al. Strong Spatiotemporal localization in a silica nonlinear waveguide Array. Phys Rev Lett 2003;91:223901.
[44] Li B-B, Zhao Y, Xu S-L, et al. Two-dimensional gap solitons in parity-time symmetry moiré optical lattices with Rydberg-Rydberg interaction. Chin Phys Lett 2023;40:044201.
[45] Bai Z, Li W, Huang G. Stable single light bullets and vortices and their active control in cold Rydberg gases. Optica 2019;6:309.
[46] Zhao Y, Lei Y-B, Xu Y-X, Xu S-L, Triki H, Biswas A, et al. Vector spatiotemporal solitons and their memory features in cold Rydberg gases. Chin Phys Lett 2022;39:034202.
[47] Guo Y-W, Xu S-L, He J-R, Deng P, Belić MR, Zhao Y. Transient optical response of cold Rydberg atoms with electromagnetically induced transparency. Phys Rev A 2020;101:023806.
[48] Liao Q-Y, Hu H-J, Chen M-W, et al. Two-dimensional spatial solitons in optical lattices with Rydberg-Rydberg interaction. Acta Phys Sin 2023;72:104202.
[49] Armstrong JA, Bloembergen N, Ducuing J, Pershan PS. Interactions between light waves in a nonlinear dielectric. Phys Rev 1962;127:1918.
[50] Skorobogatiy M, Yang J. Fundamentals of photonic crystal guiding. Cambridge, England: Cambridge University Press; 2009.
[51] Kong C, Li J, Tang X, Li X, Jiao J, Cao J, Deng H. Composite solitary vortices of three-wave mixing in quasi-phase-matched photonic crystals. Chaos Solitons Fractals 2024;187:115358.
[52] Zhao F, Xu X, He H, Zhang L, Zhou Y, Chen Z, Malomed BA, Li Y. Vortex solitons in quasi-phase-matched photonic crystals. Phys Rev Lett 2023;130:157203.
[53] He J-R, Jiao Y, Zhou B, Zhao Y, Fan Z, Xu S. Vortex light bullets in rotating Quasi-Phase-Matched photonic crystals. Chaos Solitons Fractals 2024;188:115514.

[54] Arie A, Voloch N. Periodic, quasi-periodic, and random quadratic nonlinear photonic crystals. Laser & Photonic Rev 2010;4:355.
[55] H Li, Ma B. Research development on fabrication and optical properties of nonlinear photonic crystals. Front Optoelectron 2020;13:35.
[56] Hatanaka T, Nakamura K, Taniuchi T, Ito H, Furukawa Y, Kitamura K. Quasi-phase-matched optical parametric oscillation with periodically poled stoichiometric LiTaO3. Opt Lett 2000;25:651.
[57] Chowdhury A, Ng HM, Bhardwaj M, Weimann NG. Second-harmonic generation in periodically poled GaN. Appl Phys Lett 2003;83:1077.
[58] Xu T, Switkowski K, Chen X, Liu S, Koynov K, Yu H, Zhang H, Wang J, Sheng Y, Krolikowski W. Three-dimensional nonlinear photonic crystal in ferroelectric barium calcium titanate. Nat Photonics 2018;12:591.
[59] Keren-Zur S, Ellenbogen T. A new dimension for nonlinear photonic crystals. Nat Photonics 2018;12:575.
[60] Agrawal GP. Nonlinear fiber optics. fifth ed. New York: Academic Press; 2013.
[61] Mihalache D, Mazilu D, Malomed BA, Torner L. Walking light bullets. Opt Commun 1999;169:341–56.
[62] Mihalache D, Mazilu D, Crasovan L-C, Torner L, Malomed BA, Lederer F. Three-dimensional walking spatiotemporal solitons in quadratic media. Phys Rev E 2000;62:7340.
[63] Torner L, Mazilu D, Mihalache D. Walking solitons in quadratic nonlinear media. Phys Rev Lett 1996;77:2455.
[64] Etrich C, Peschel U, Lederer F, Malomed BA. Stability of temporal chirped solitary waves in quadratically nonlinear media. Phys Rev E 1997;55:6155.
[65] Mihalache D, Mazilu D, Crasovan L-C, Towers I, Malomed BA, Buryak AV, Torner L, Lederer F. Stable three-dimensional spinning optical solitons supported by competing quadratic and cubic nonlinearities. Phys Rev E 2002;66:016613.
[66] Hayata K, Koshiba M. Multidimensional solitons in quadratic nonlinear media. Phys Rev Lett 1993;71:3275.
[67] Malomed BA, Drummond P, He H, Berntson A, Anderson D, Lisak M. Spatiotemporal solitons in multidimensional optical media with a quadratic nonlinearity. Phys Rev E 1997;56:4725.
[68] Mihalache D, Mazilu D, Dörring J, Torner L. Elliptical light bullets. Opt Commun 1999;159:129–38.
[69] Porras MA. Upper bound to the orbital angular momentum carried by an ultrashort pulse. Phys Rev Lett 2019;122:123904.
[70] Karnieli A, Arie A. Fully controllable adiabatic geometric phase in nonlinear optics. Opt Express 2018;26:4920–32.
[71] Xu X, Zhao F, Huang J, He H, Zhang L, Chen Z, Nie Z, Malomed BA, Li Y. Semidiscrete optical vortex droplets in quasi-phase-matched photonic crystals. Opt Express 2023;31:38343–54.
[72] Zhang Y, Sheng Y, Zhu S, Xiao M, Krolikowski W. Nonlinear photonic crystals: from 2D to 3D. Optica 2021;8:372–81.
[73] Li Y, Pang W, Malomed BA. Nonlinear modes and symmetry breaking in rotating double-well potentials. Phys Rev A 2012;82:063813.
[74] Li Y, Pang W, Malomed BA. Nonlinear modes and symmetry breaking in rotating double-well potentials. Phys Rev A 2012;86:023832.
[75] Huang H, Lyu L, Xie M, Luo W, Chen Z, Luo Z, Huang C, Fu S, Li Y. Spatiotemporal solitary modes in a twisted cylinder waveguide shell with the self-focusing Kerr nonlinearity. Commun Nonlinear Sci Numer Simul 2019;67:617–26.
[76] Hu X, Zhang Y, Zhu S. Nonlinear beam shaping in domain engineered ferroelectric crystals. Adv Mater 2020;32:1903775.
[77] Liu S, Wang L, Mazur LM, Switkowski K, Wang B, Chen F, Arie A, Krolikowski W, Sheng Y. Highly efficient 3D nonlinear photonic crystals in ferroelectrics. Adv Optical Mater 2023;11:2300021.
[78] Porat G, Arie A. Efficient, broadband, and robust frequency conversion by fully nonlinear adiabatic threewave mixing. J Opt Soc Am B 2013;30:1342.
[79] Luther GG, Alber MS, Marsden JE, Robbins JM. Geometric analysis of optical frequency conversion and its control in quadratic nonlinear media. J Opt Soc Am B 2000;17:932.
[80] Yang J, Lakoba TI. Accelerated imaginary-time evolution methods for the computation of solitary waves. Stud Appl Math 2008;120:265–92.
[81] Michinel H, Salgueiro JR, Paz-Alonso MJ. Square vortex solitons with a large angular momentum. Phys Rev E 2004;70:066605.
[82] Chen S, Zhou B, Jiao Y, Wang L, Zhao Y, Xu S. Vortex solitons in rotating quasi-phase-matched photonic crystals. Opt Express 2024;32:39963–73.
[83] Vakhitov NG, Kolokolov AA. Stationary solutions of the wave equation in a medium with nonlinearity saturation. Radiophys Quantum Electron 1973;16:783.
[84] Huang C, Ye Y, Liu S, He H, Pang W, Malomed BA, Li Y. Excited states of two-dimensional solitons supported by spin–orbit coupling and field-induced dipole–dipole repulsion. Phys Rev A 2018;97:013636.
[85] Dmitriev VG, Gurzadyan GG, Nikogosyan DN. Nonlinear optical properties of crystals. Handb Nonlinear Opt Cryst 1991;64:53–127.
[86] Ganeev RA, Kulagin IA, Ryasnyanskii AI, Tugushev RI, Usmanov T. The nonlinear refractive indices and nonlinear third-order susceptibilities of quadratic crystals. Opt Spectrosc 2003;94:561–8.
[87] Buryak AV, Trapani PD, Skryabin DV, Trillo S. Optical solitons due to quadratic nonlinearities: From basic physics to futuristic applications. Phys Rep 2002;63:370.